doi:10.14311/ppt.2025.2.117
Plasma Physics and Technology **12**(2):117–122, 2025

USE OF OPTICAL METHODS FOR TEMPERATURE EVALUATION OF SWITCHING CuCr CONTACTS IN VACUUM

S. Gortschakow[a,*], G. Gött[a], R. Methling[a], D. Uhrlandt[a], N. Dorraki[b], A. Lawall[b], F. Graskowski[b]

[a] *Leibniz Institute for Plasma Science and Technology, Felix-Hausdorff-Straße 2, 17489 Greifswald, Germany*

[b] *Siemens AG, Rohrdamm 88, 13629 Berlin, Germany*

[*] sergey.gortschakow@inp-greifswald.de

Abstract. Properties of switching vacuum arcs are affected by melting and evaporation of the electrodes.The surface temperature dynamics during high-current operation was studied for the case of cylindrical contacts made of materials conventionally used for switching applications, namely CuCr40 and CuCr50. The measurements of the arc current and voltage have been accompanied by electrode temperature determination using a combination of near infrared radiation (NIR) spectroscopy and high-speed camera imaging enhanced by narrow-band filter. Special attention was put on the cooling dynamics of cathode and anode after current interruption. Lower thermal conductivity of CuCr alloy with higher Cr content leads to longer temperature decay. Faster cooling of the cathode surface comparing to the anode due to better current density distribution and moving of attachment points were found.

Keywords: vacuum arc, optical diagnostics, optical emission spectroscopy, thermography.

1. Introduction

The lifetime of the electrode system in switching applications is mainly limited by accumulated thermal load of the electrode surface. The diagnostics of the electrode surface plays, therefore, an important role for understanding of basic phenomena in arc-electrode interaction and material qualification. The right choice of the electrode material is very important for long lifetime and stable operation of switching devices. The contact surface changes its morphology when it is loaded with a high current due to melting, evaporation and solidification processes. This can affect the arc properties, like e.g. arc voltage and arc current behaviour, arc dynamics, surface temperature dynamics and erosion rate. When the arc current increases above a certain level, an arc constriction occurs. In the case of the anode-driven constriction, several high-current modes are distinguished: footpoint mode, anode spot (type 1 and type 2) and anode plume [1, 2]. In particular, the anode spot and anode plume modes cause intense material evaporation and surface degradation. In the current study, properties of switching arcs in case of constricted anode attachment were investigated. Two conventional materials, namely CuCr40 and CuCr50 (40% and 50% Cr mass fraction, correspondingly) have been studied. The measurements of the arc current and voltage have been accompanied by various optical diagnostics. The arc dynamics was observed by a high-speed camera. Near infrared radiation (NIR) spectroscopy determined the electrode surface temperature after current zero crossing. During the active phase, a high-speed camera equipped by a narrow band filter was applied for acquisition of qualitative distribution of the electrode surface radiation. Using special calibration routine, a two-dimensional time-dependent temperature evolution has been evaluated. Special attention was put on the cooling dynamics after current interruption.

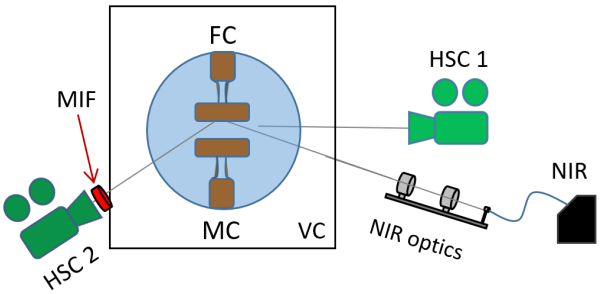

Figure 1. Schematic view of experimental setup. VC – vacuum chamber, FC - fixed contact, MC – moving contact, NIR – near-infrared spectrometer, MIF – narrow-band filter, HSC – high-speed camera.

2. Experimental setup

Experimental setup consists of a model circuit breaker, equipped with pumping system and drive for electrode movement, a power source, and diagnostic equipment. Detailed description of the setup is given elsewhere [2, 3]. Here only a brief description is presented. Schematic representation of the main part of experimental setup is shown in Fig. 1.

2.1. Model circuit breaker

The main part of the model circuit breaker is a vacuum chamber (VC in Fig. 1), which was evacuated by the pumping system below 10^{-6} mbar before every experiment. The chamber is equipped with four windows which provide optical assess for various diagnostics. Cylindrical CuCr electrodes with a diameter of 22 mm were used (Fig. 9). The upper electrode (FC) is fixed and connected to a power source while the lower electrode (MC) was a moveable grounded one. The pneumatic drive provided an average velocity of about 1.25 m/s. The arc ignition occurs by electrode separation during the current flow. A 50 Hz damped AC high-current generator based on capacitor bank provided the peak current up to 4500 A.

2.2. Diagnostics

Synchronised electrical and optical measurements were applied. The arc current and voltage were measured by a Rogowski coil (PEM CWT 1500) and a voltage probe (Tektronix P6015A, bandwidth 75 MHz), correspondingly. A high-speed camera (Photron Nova S12, HSC 1 in Fig. 1) is used for the registration of general arc dynamics. Temporal evolution of the anode surface temperature was determined from combined measurements by a high-speed camera (Photron Nova S6, HSC 2 in Fig. 1) equipped with a narrow band filter (MIF in Fig. 1, central wavelength 891 nm, FWHM 10 nm) and a compact NIR spectrometer (Hamamatsu C114GA, NIR in Fig. 1). The parameters of filter are chosen to minimize the contribution of plasma radiation during the measurements of contact surface temperature. The NIR spectrometer and camera HSC 2 are positioned at the same viewing angle of about 16^o to the anode surface. A focusing optical system (NIR optics in Fig. 1) images a region of about 3 mm^2 in the area where the anode spot was expected on the entrance slit of the NIR spectrometer (Fig. 2). The NIR spectrometer provides a temporal resolution of 1.25 ms. Its exposure time was set to 100 µs. The high-speed camera acquires the images with 22500 fps with typical exposure time of 5 µs. The spectra recorded by the NIR spectrometer are processed by comparing the measured spectral radiances to the black body emission according to Planck law [2–4]. Figure 3 shows an example of spectra acquired at two time instants during one experiment, namely during the active phase (t = 7.9 ms) and after arc termination (t = 11.35 ms). At earlier time instants $t < 9.5$ ms, the contribution of plasma radiation is visible through the pronounced line radiation from the electrode materials Cu (985, 1005, 1600 nm) and Cr (957 and 1160 nm). The continuum part coming from plasma is also present, but its contribution is usually below 10%.

Prior to temperature evaluation, each spectrum has to be subjected to special calibration routine.

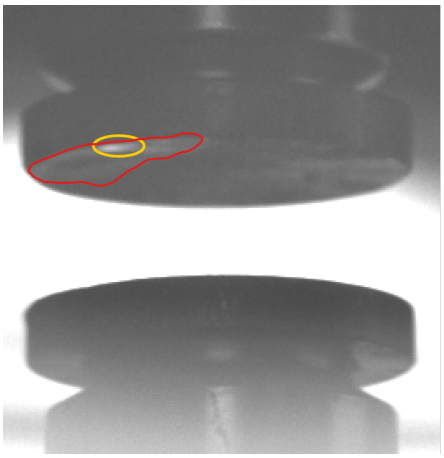

Figure 2. Example of NIR optics focussing. Red line adumbrates the area at which the anode spot is expected, yellow ellipse marks the laser position.

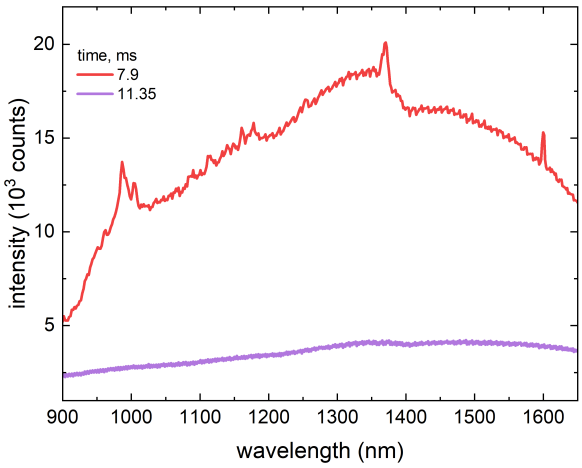

Figure 3. Example of NIR spectra acquired during one experiment. Red line (7.9 ms) during arcing, violet line (11.35 ms) - after current interruption.

First, the dark spectrum has to be subtracted. Then, the spectrum has to be corrected by transmission (Fig. 4), which is dependent on the level of window blackening. It was assumed, that the transmission changes linearly in dependency on transferred charge, i.e. in the each subsequent experiment the shape of transmission curves remains but the absolute value decreases according to the total transferred charge from all previous experiments with the same protecting window. Further correction appears due to the specific sensitivity of NIR detector. Figure 5 presents the signal of calibration source and its registration by spectrometer. The corresponding relation between two curves is taken into account for evaluation. As the result, a spectral radiance in units [W/m^2/nm/sr] from each spectrum is derived. Figure 6 shows an example of acquired an calibrated spectra.

After calibration each spectrum was compared with the spectral radiance of a black body according to

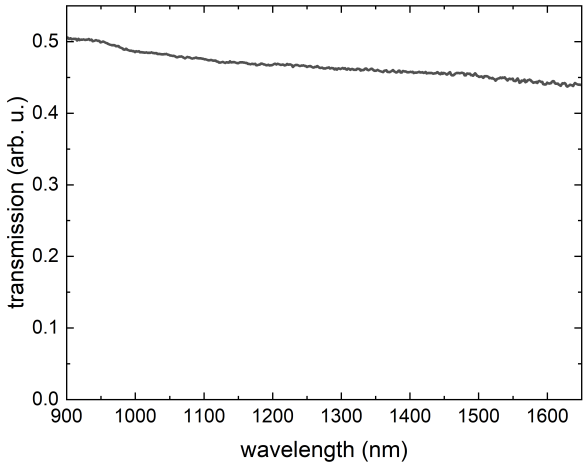

Figure 4. Example of transmission curve.

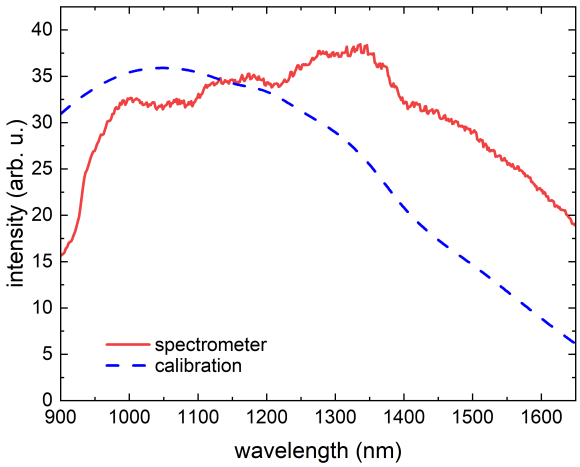

Figure 5. Comparison of measured NIR spectrum (red full line, "spectrometer") with data for calibration source (blue dashed line, "calibration").

Planck law corrected by surface emissivity $\varepsilon(\lambda, T)$.

$$B_\lambda(\lambda, T) = \varepsilon(\lambda, T)\frac{2hc^2}{\lambda^5}\frac{1}{\mathrm{e}^{-\mathrm{hc}/\lambda \mathrm{k_B T}} - 1} \qquad (1)$$

Here, h is the Planck constant, k_B - Boltzmann constant, c - speed of light, λ - the wavelength and T is the surface temperature. In the assumption of wavelength independent emissivity $\varepsilon(\lambda, T) = \varepsilon(T)$, the temperature influences solely the shape of the curve B_λ, while the absolute values are given by the emissivity. Thus, both values T and ε can be determined form two parameter fit [4]. Figure 7 shows examples of Planck fits for the instants during the active phase and after current termination. The best fit is given by combinations $(T, \varepsilon) = (2397 \pm 12\,\mathrm{K}, 0.36 \pm 0.01)$ and $(1931 \pm 7\,\mathrm{K}, 0.19 \pm 0.005)$ for 7.9 and 11.35 ms, correspondingly.

The correlation between arc intensity, recorded by high-speed camera, and surface temperature, measured by the NIR spectrometer, is utilized to determine the anode surface temperature during the active phase. The detector of the camera just can

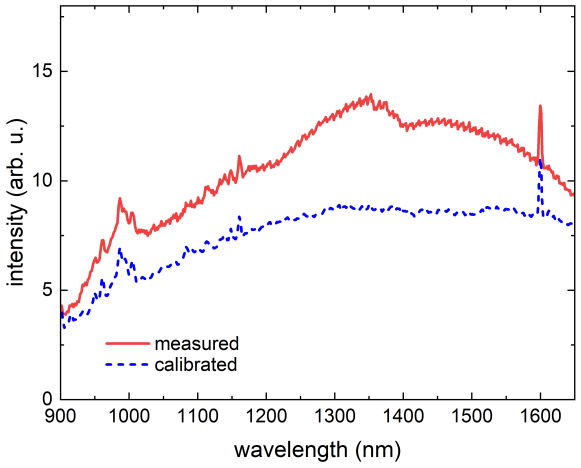

Figure 6. Example of measured NIR spectrum before (full red line) and after (dashed blue line) calibration routine.

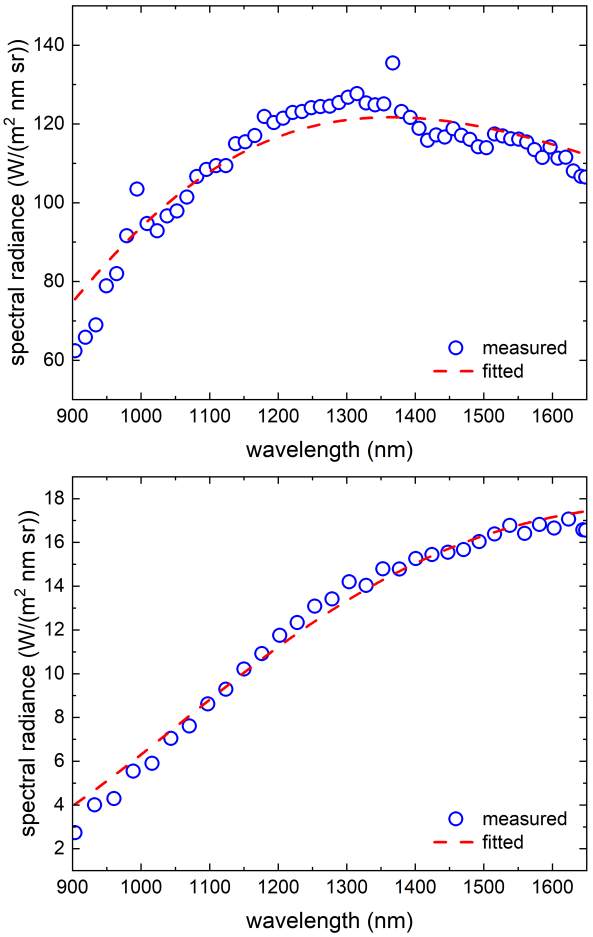

Figure 7. Example of Planck fit (line) for calibrated NIR spectra (symbols). Instants 7.9 ms (upper part) and 11.35 ms (lower part) (cf. Fig. 3).

see radiation at wavelengths that are transmitted by the metal interference filter. Due to rather narrow bandwidth of the filter, it can be assumed that the detector sensitivity is constant in the relevant wavelength range. Hence, the measured intensity is proportional to the integral over the transmission

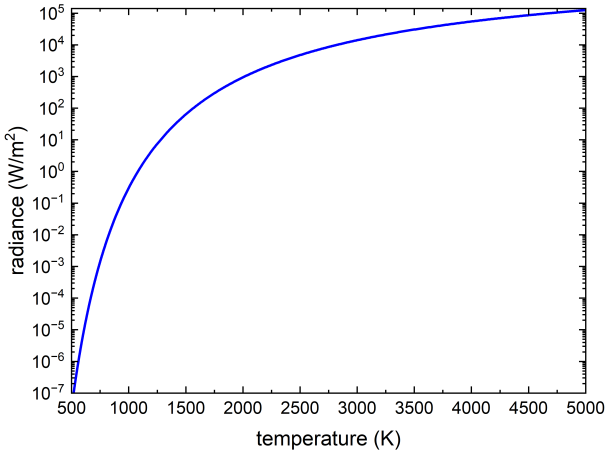

Figure 8. MIF-filtered radiance for used 890 nm filter.

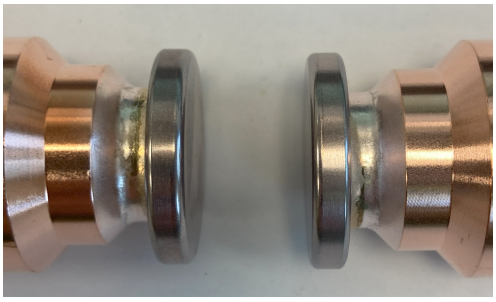

Figure 9. Image of electrodes used in the study.

function multiplied with the Planck function $L_{\mathrm{MIF}}(T)$

$$L_{\mathrm{MIF}}(T) = \int_{\lambda} P_{\mathrm{MIF}}(\lambda) B_{\lambda}(\lambda, T) d\lambda \qquad (2)$$

$P_{\mathrm{MIF}}(\lambda)$ is the transmission function of the metal interference filter, which could be determined experimentally or is given by the manufacturer. . In the case of used filter, the MIF-filtered radiance is shown in Fig. 8. When it is not possible to measure the MIF-filtered radiance in absolute units, an additional method for determination of the absolute temperature is required. The radiance measured in arbitrary units can be related to the temperature by fixation of MIF-filtered signal intensity. The measurements have to be performed for the region of NIR measurements and at the same instants as for NIR spectroscopy. Measured signal intensity is, then, calibrated to the curve shown in Fig. 8. As it is obvious from Fig. 8, large variation of radiance lead to small variation in the temperature only. Thus, in the temperature region 1500–2100 K the change of radiance by 50% causes the deviation in the temperature value by about 5% only. This makes the method robust against possible non-linearity of used camera detector. Further details of the method, like e. g. calibration routine, possible restrictions, handling in special case of intense arc radiation, can be found in [2–4].

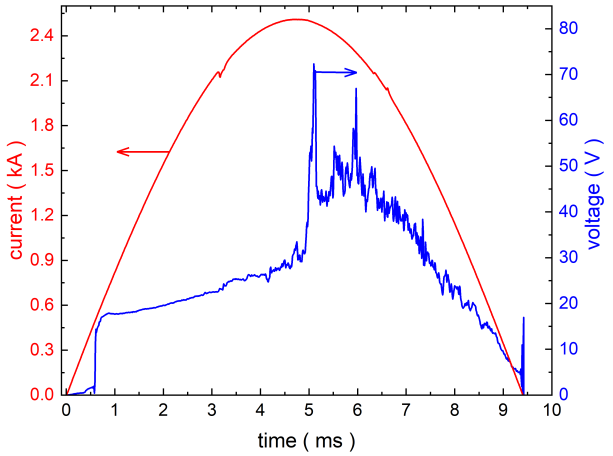

Figure 10. Example of evolution of arc voltage (blue line) and arc current (red line). Peak arc current 2.5 kA, arc duration 9 ms, electrode material CuCr40.

3. Results and discussion

3.1. Electrical properties

Figure 10 presents the typical evolution of arc current and arc voltage in the case of pronounced anode activity. The arc ignition is accompanied by a voltage jump of about 15 V at $t = 0.6$ ms. For the next 3 ms the arc plasma remains diffuse. Small voltage fluctuations between 4 and 5 ms are related to the transition to the footpoint mode. Stable anode spot appears at $t = 4.8$ ms. Its formation is accompanied by a significant voltage jump. The anode spot position is slightly changing leading to voltage oscillations. Higher voltage peaks correspond to stronger shift of anode spot position.

3.2. Anode temperature evolution during the active phase

Used optical diagnostics allows for determination of time-dependent two-dimensional distribution of the anode surface temperature. The method [3] requires a combination of spectrally filtered high-speed imaging with evaluation of NIR spectra. The latter is used for calibration of acquired two-dimensional surface radiation. An example of maximum anode temperature is shown in Fig. 11. A good agreement between both methods is obvious. Thus, the reliability of calibration procedure is confirmed.

Figure 12 presents selected spectrally filtered images of surface radiation and reconstructed temperature distribution close after the instant of anode spot formation ($t = 4.9$ ms in Fig. 10). Anode is on the top. Cathode spots are visible on the lower electrode. The anode spot radiation is fluctuating due to the spot activity which lead to variation of temperature distribution. The temperature temporarily decreases from about 2500 K ($t = 4.9$ ms) to about 2050 K ($t = 5.5$ ms). In contrast to recent study [5], no pronounced spot-to-plume transitions were observed.

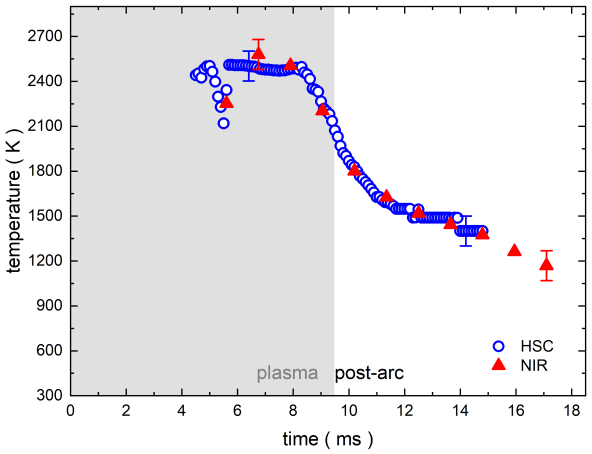

Figure 11. Evolution of maximum anode surface temperature determined by HSC measurements (blue circles) and NIR measurements (red triangles). Gray zone shows the period where arc plasma exists. Error bars show the method uncertainty acc. to [4]. Electrode material CuCr40, arc duration 9 ms.

The temperature variation appears due to spot instability only. Nevertheless, the temperature drop is accompanied by a voltage fall of about 30 V. A subsequent temperature rise at $t = 5.7$ ms is accompanied by a voltage jump of about 12 V. Similar correlation between the voltage and anode surface temperature was found in [5].

3.3. Temperature measurements after current interruption

Changes in the surface morphology of the electrode and amount of melted material after current interruption depends among others on the surface cooling dynamics. Figure 13 shows temperature decay in the hottest point of anode close and after the instant of current interruption (CZ - current zero crossing point). The values have been evaluated from several shots. The error bars show, therefore, the shot-to-shot variation of the temperature in the region of measurements. The temperature of anode melted area reaches about 2500 K before current zero (grey marked zone in Fig. 13). In the case of anode spot formation, this value is comparable for both materials. After current termination CuCr40 shows slightly lower temperature comparing to CuCr50. Furthermore, in case of CuCr40, the anode surface approaches 1000 K at about 10 ms after current interruption. The material with higher Cr content reach this point later, at about $t = 14$ ms. The cooling for the material with higher Cr content takes in general longer time. The reason for this is the lower thermal conductivity which leads to slower heat dissipation in the electrode bulk.

The diagnostics of the cathode surface temperature is much complicated comparing to that of the anode. The cathode attachment consists of many fast moving spots (cf. Fig. 12, lower part of images in the left column). During the arc phase,

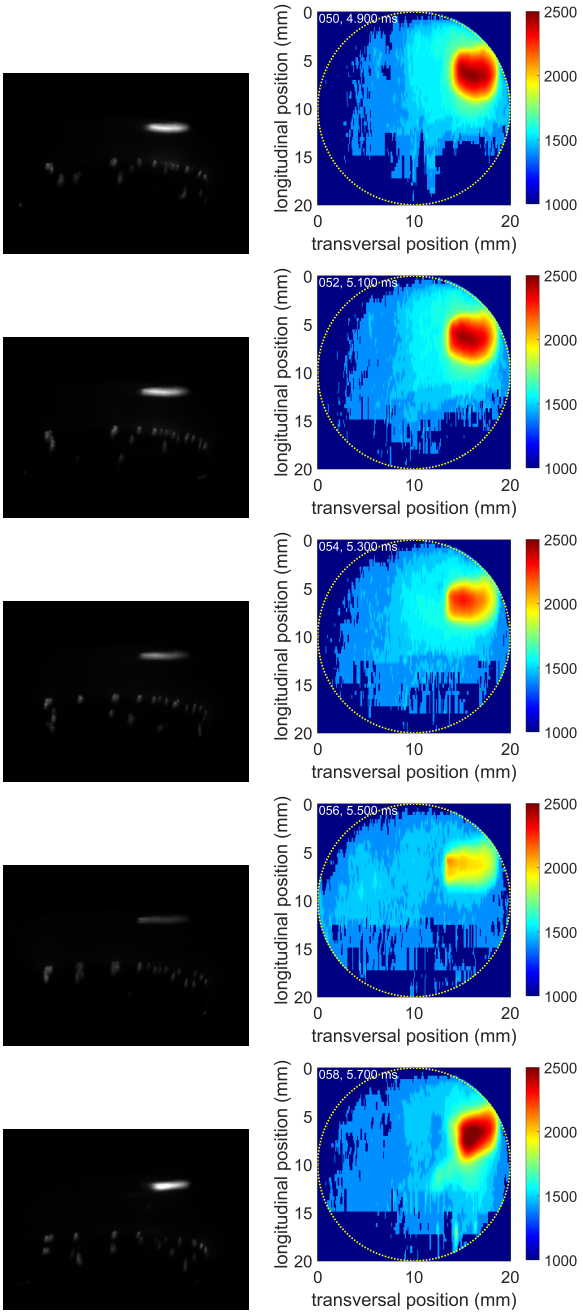

Figure 12. Evolution of anode surface temperature determined by HSC measurements. Left column - spectrally filtered image of the (top - anode, bottom - cathode); right column - reconstructed surface temperature. First image $t = 4.9$ ms, time step 0.2 ms. Electrode material CuCr40, peak arc current 2.5 kA, arc duration 9 ms.

those spots stochastically cross the position of measurements leading to strong variation of signals acquired by high-speed camera and NIR spectrometer. The cathode spots disappear close before current interruption. Thus, NIR signal is usually missing after current zero. In some cases, however, the surface emits sufficient light for its diagnostics. The cathode surface was hot enough in case of CuCr50 electrodes. An example of cathode surface temperature decay after

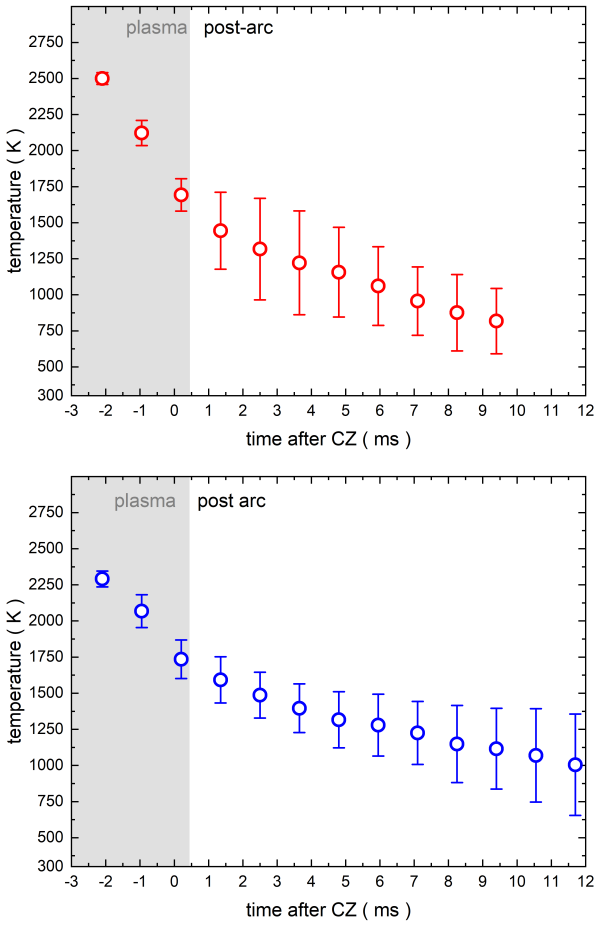

Figure 13. Maximum anode temperature determined for CuCr40 (upper part) and CuCr50 (lower part) electrodes with anode spot mode. Gray zone shows the period where arc plasma exists. Arc duration 9 ms.

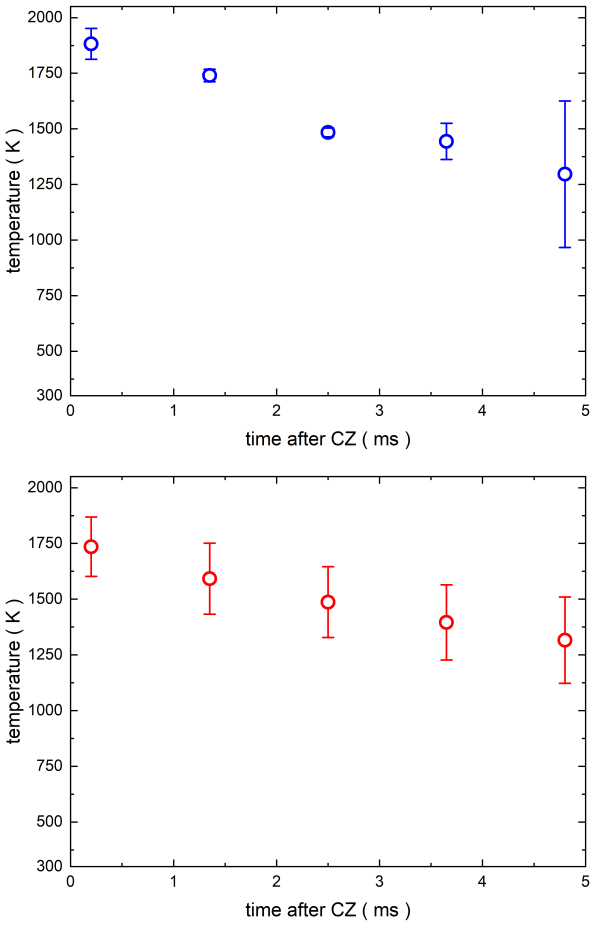

Figure 14. Maximum temperature of the cathode (upper part) and anode (lower part) made of CuCr50 material after current interruption. Peak arc current 4.2 kA, arc duration 9 ms.

current termination is shown in Fig. 14 along with the data for anode at similar experimental conditions. The temperature of cathode diminishes rapidly. After about 5 ms, its value amounts to 1000 K. At the same instant, the anode surface temperature is about 1520 K. The reasons for this difference are a constricted attachment and fixed spot position at the anode. The shot-to-shot variation shown by error bars is smaller in case of cathode, as the moving spots ensure more homogeneous temperature distribution.

4. Conclusions

Optical diagnostics was used for determination of electrode surface temperature of switching CuCr contacts in vacuum. The temperature evaluation of the anode surface was possible both in the arc and post-arc phase, while the cathode was accessible in the post-arc phase only. Higher Cr content leads to deceleration of surface cooling after current interruption. More homogeneous current distribution over the cathode surface and fast moving cathode spots promote faster temperature decay of the cathode comparing to the anode.

References

[1] H. C. Milner. Vacuum arcs. *IEEE Trans. Plasma Sci.*, 51:1585–1594, 2023. doi:10.1109/TPS.2023.3261779.

[2] S. Gortschakow. Diagnostic methods for switching vacuum arcs based on high-speed camera technique. *IEEE Trans. Plasma Sci.*, 52:4382–4389, 2024. doi:10.1109/TPS.2024.3353826.

[3] S. Gortschakow, S. Franke, R. Methling, et al. Advanced optical diagnostics for characterization of arc plasmas. *IEEE Trans. Plasma Sci.*, 49:2505–2515, 2021. doi:10.1109/TPS.2021.3096289.

[4] R. Methling, S. Franke, S. Gortschakow, et al. Anode surface temperature determination in high-current vacuum arcs by different methods. *IEEE Trans. Plasma Sci.*, 45:2099–2107, 2017. doi:10.1109/TPS.2017.2712562.

[5] N. Dorraki, R. Methling, and S. Gortschakow. Advanced temporal analysis of anode activity during mode transitions in high current vacuum arcs. *J. Phys. D: Appl. Phys.*, 58:075204, 2025. doi:10.1088/1361-6463/ad96c5.